Antibacterial activity, photocatalytic and magnetic properties of Fe_3O_4 nanoparticles prepared by simple combustion method

S. Rosy Christy [1,2*], G. Padma Priya [3], N. Babitha [1], S. Arunadevi [1]

[1] Department of Chemistry, Urumu Dhanalakshmi College, Tiruchirappalli 620019, Tamil Nadu, India

[2] Department of Chemistry, PERI Institute of Technology, Mannivakkam, Chennai 600048, India

[3] Department of Chemistry, Bharath Institute of Higher Education and Research, Bharath University, Chennai – 600 073, Tamil Nadu, India

Corresponding author's e-mail: prwwwprcom47@gmail.com

Abstract

Magnetic Fe_3O_4 nanoparticles (FENPs) and nanorods (FENRs) were employed to prepare facile techniques such as microwave and conventional combustion methods respectively using aloe vera as the bio-reducing agent. The as-synthesized FENPs and FENRs were characterized using X-ray diffraction (XRD), High resolution scanning electron microscopy (HR-TEM), Energy dispersive X-ray (EDX), Fourier transform infrared spectra (FT-IR), Diffuse reflectance spectroscopy (DRS) and Vibrating sample magnetometer (VSM) techniques. The optical absorption of FENPs and FENRs was extended into visible region. The magnetic property of the FENPs and FENRs prescribes it to be easily separable material for reusability in photocatalytic application. The catalytic activity of the prepared FENPs and FENRs was evaluated based on the

photo-degradation of methylene blue (MB). FENPs sample depicted good photocatalytic activity due to extended photo-responsive range and increase in charge separation rate. From the results we suggest that the attractive physical properties and efficient catalytic active NPs has been used as promising photocatalyst under UV light irradiation for high efficiency and recyclability for practical use in wastewater treatment to control water pollution.

Keywords: Photo-degradation; Methylene blue; Magnetic nanoparticles; Recyclability.

1. Introduction

Semiconductor magnetic nanoparticles (SMNPs) containing more different functionalities can show novel physico-chemical properties, which will be essential for future technological applications. They are used as an effectual technique to eliminate pollutants from wastewater and air, due to their exclusive magnetic, optical and electronic properties [1-2]. In recent years, the treatment for dye degradation of varied industrial effluents has become a necessary topic within the analysis field to regulate the environmental pollution. Advance oxidation processes (APO) such as photocatalysis has attracted remarkable interest because it offers a sustainable pathway to drive chemical reactions such as water splitting carbon fixation and organic pollutants degradation [3-5].

Magnetic Fe_3O_4 nanoparticles are widely used, not only as information storage ferrofluids and position sensing, but also used as promising aspirant for biomolecule imaging (BMI), catalytic separation and sensing [6-8]. Fe_3O_4 nanoparticles is an n-type semiconductor that has been applied in many applications like chemical sensor for many molecules, photoelectrode in solar cells with its unique photoelectric property [9-11], chemical stability, and

non toxicity it is used as a potential catalyst for photocatalytic application. Researchers in the last decades have been focused on the use of semiconductors as photocatalyst [12-14].

Fe_3O_4 nanoparticles have many necessary issues for photocatalytic application. Behind the photocatalytic reaction, the process of splitting the photocatalyst material from dye waste is crucial [15]. The electron and hole pairs recombination rate are too rapid. The high rate recombination electron holes pairs and reusability limitation of that semiconductor could limit the efficiency as a catalyst [16]. To conquer the problem, one strategy has been adopted to make magnetically separable photocatalyst (MSP) for reuse and recovery of Fe_3O_4 nanoparticles [17].

Chen et al. [18] has prepared different morphologies of Fe_3O_4 including octahedrons, sheets, and irregularly shaped particles using different concentration of NaOH by a simple hydrothermal method. Srivastava et al. [19] prepared superparamagnetic Fe_3O_4 nanoparticle and Fe_3O_4/alginate nanocomposites (NCs) were synthesized by co-precipitation, and in situ co-precipitation assisted polymerization methods, respectively, and they have reported that the value of saturation magnetization in case of Fe_3O_4/alginate NCs decreases by increasing the pH value. Roychowdhury et al. [20] synthesized Fe_3O_4/ZnO NCs by ultrasonication of the constituents prepared separately by the wet chemical routes. The magnetization measurements show that the saturation magnetization (M_s) decreases with increase in ZnO content in the NCs, which is explained as due to the reduction of strength of dipolar interaction among Fe_3O_4 nanoparticles, and also due to the inclusion of diamagnetic ZnO. Zhang et al. [21] also have prepared Fe_3O_4 nanoparticles by autoclave method at 200 °C for 12 h.

Some of the methods used are hydrothermal, solvothermal, co-precipitation, microwave assisted method, electrodeposition, thermal evaporation and sol-gel process [11-15]. Recently, the biosynthetic method (BSM) employs the plant extracts, which have emerged as a simple and

viable alternative to the chemical synthetic procedures and physical methods. Nanomaterial synthesis using the microorganisms, enzymes, and plant extracts has been suggested as the possible eco-friendly alternatives to phytosynthesis. The biosynthetic route is very simple and provides high-yield nanomaterials with well crystalline structure and acceptable properties. Generally, Aloe vera (*Aloe barbadensis mill*.) is a perennial succulent belonging to the *Liliaceal* family, and it is a cactus-like plant that grows in hot, dry climates. Aloe vera gel is a colorless and present in the inner part of the fresh leaves. However, Aloe vera has been reported to possess anti-inflammatory, UV protective, antiprotozoal and wound- and burn-healing promoting properties [22-25]. Aloe vera extract provides a simple, efficient, and green route for the synthesis of nanomaterials. Moreover, many research groups have also reported the use of Aloe vera plant extract for the synthesis of various nanomaterials [26-31]. In the present study, we have synthesized magnetic FENPs and FENRs by combustion methods using urea as the bio-reducing agent. Owing to the more cost-effective and composed process provides a promising route for the controlled synthesis of magnetic Fe_3O_4 nanoparticles. Moreover, the magnetic properties and photocatalytic application of the Fe_3O_4 nanoparticles were investigated.

2. Experimental

2.1 Synthesis of Fe_3O_4 (FENPs and FENRs) nanostructures

The chemical used in this study were of analytical grade obtained from Merck, India and were used as received without further purification. Ferric nitrate ($Fe(NO_3)_3 \cdot 9H_2O$, 98%) and Aloe vera extract as the raw materials were used for these methods. The Aloe vera leaves were collected from the local agricultural fields, Peravurani, Thanjavur District, Tamil Nadu State, India. Aloe vera extract was prepared from a 5 g portion of thoroughly washed Aloe vera leaves

were finely cut and the gel obtained was dissolved in 10 ml of de-ionized water and stirred for 30 min to obtain a clear solution. The resulting product was used as an Aloe Vera extract.

Ferric nitrate (10 mmol) was first dissolved in the Aloe vera extract under vigorous stirring at room temperature for 1 h until a clear transparent solution was obtained. In this preparation process, Aloe vera extract has a double function of both reducing and gelling agent for the synthesis of mixed metal oxides. Metal nitrate salts and the Aloe vera extract were chosen by considering the total reducing and oxidizing agent valences of the raw materials and were quantified in equivalence of NOx reduction (N_2O to N_2, CO_2 and H_2O) at a low temperature. The precursor mixture of metal nitrates in Aloe vera extracted solution was placed in a domestic microwave oven and exposed to the microwave energy in a 2.45 GHz multimode cavity at 850 W for 10 min. Initially, the precursor mixture boiled and underwent evaporation followed by the decomposition with the evolution of gases. When the solution reached the point of spontaneous combustion, it vaporized and instantly became a solid. After completion of the reaction, the obtained solid powder was then washed with ethanol and dried at 70 ºC for 1h. The obtained powders were labeled as Fe_3O_4 (FENPs) which was obtained by MCM approach.

The another part of the solution mixture was taken in the silica crucible and was placed in an air furnace and sintered at 500 °C at a heating rate of 5 °C/min for 2 h. Initially, the solution was boiled and dehydrated followed by decomposition with the evolution of gases. It vaporized the solution and slowly became a solid. After completion of the reaction, the obtained solid powder was then washed with ethanol and dried at 70 ºC for 1h. The obtained powders were labeled as Fe_3O_4 (FENRs), prepared by CCM technique.

2.2. Characterizations

Structural characterization of nanocrystalline Fe_3O_4 powders (FENPs and FENRs) was performed using a Rigaku Ultima IV high resolution powder X-ray diffractometer (XRD) with CuKα radiation at $\lambda = 1.5418$ Å. The surface functional groups were analyzed by Perkin Elmer FT-IR spectrometer. Morphological studies and elemental chemical analysis have been performed with a Jeol JSM6360 high resolution scanning electron microscope (HR-SEM) equipped with energy dispersive X-ray (EDX) analysis. The transmission electron micrographs were carried out by Philips-TEM (CM20). The UV-visible diffuse reflectance spectrum (DRS) was recorded using Cary100 UV-Visible spectrophotometer to estimate their band gap energy. Magnetic measurements were carried out at room temperature using a PMC MicroMag 3900 model vibrating sample magnetometer (VSM) equipped with 1 Tesla magnet.

2.3. Photocatalytic reactor setup and degradation procedure

All photochemical reactions under identical conditions were carried out in a self-designed photocatalytic reactor. This model consists of eight medium pressure mercury vapor lamps (8W) set in parallel and emitting 365 nm wavelength. It has a reaction chamber with specially designed reflectors made of highly polished aluminium and built in cooling fan at the bottom and black cover to prevent UV leakage. It is provided with the magnetic stirrer at the center. Open borosilicate glass tube of 40 cm height and 12.6 mm diameter was used as a reaction vessel. The irradiation was carried out using only six parallel medium pressure mercury lamps. The solution was aerated continuously by a pump to provide oxygen and for the complete mixing of solution. Prior to photocatalytic experiments, the adsorption of methylene blue (MB) on nano photo-catalyst was carried out by mixing 100 ml of aqueous solution of MB with fixed weight of the respective photo-catalyst. The PCD was carried out by mixing 100 ml of aqueous MB solution

and fixed weight of nano photo-catalyst FENPs and FENRs samples. All solutions prior to photolysis were kept in dark by covering with aluminium foil to prevent any photochemical reactions.

2.4. Antibacterial activity

Antimicrobial activity of the prepared samples was tested in both gram-negative and gram-positive bacteria namely *Staphylococcus aureus*, *Proteus mirabilis*, S*almonella typhii* and *Bacillus subtilis* by disc diffusion method with smaller modifications. The 24h bacterial cultures were swabbed in a Muller Hinton agar amended plates. Whatmann filter paper discs of 3 mm diameter were impregnated with 100 μL of the solution containing FENPs and FENRs samples and these discs could evaporation for 1 h. Reference standard discs were prepared with ampicillin (10 μg/mL) to compare the antibacterial activity of the samples. After drying, the discs were placed in swabbed bacterial plates and incubated at 28 °C for 24h. After incubation, plates were examined for clear zone around the discs. A clear zone more than 2 mm in diameter was taken for antibacterial activity.

3. Result and discussion

3.1. Powder X-ray diffraction analysis

Fig. 1a,b shows the powder X-ray diffraction pattern of FENPs and FENRs samples respectively. The crystallite size and structure of the prepared sample was confirmed using XRD. The diffraction peaks at $2\theta = 30.23°$, 35.54°, 43.12°, 57.25° and 62.52° can be indexed to miller indices (220), (311), (400), (511) and (440) of cubic inverse spinel structure of Fe_3O_4 lattice parameters $a = b = c$ =8.381 Å. This pattern matches with JCPDS No 85-1436 [32]. No impurity peaks with different phases were detected. Hence, the XRD pattern confirms the formation of FENPs and FENRs samples [32]. The Scherrer formula was used to calculate the crystallite size

of FENPs and FENRs samples on the basis of the (311) diffraction peak of Fe_3O_4. Using Debye Scherrer equation the crystallite size of FENPs and FENRs samples was determined.

$$d = \frac{K\lambda}{\beta cos\Theta}$$

Where d is the average crystallite size (nm), K is the grain shape factor (0.9), λ is the X-ray wavelength (nm), β is the line broadening at half the maximum intensity in radians, and Θ is the Bragg diffraction angle of the 2Θ peak. The crystallite sizes derived from FWHM of the intense peaks are shown in Table 1.

3.2 Fourier Transform Infrared Analysis

The functional group characteristics of the samples were investigated using FT-IR spectra are shown in Fig. 2. The broad absorption band observed at 3424 cm^{-1} and 3452 cm^{-1} corresponds to the O-H stretching vibrations of water molecules present in FENPs and FENRs samples [33]. The absorbance band at 1635 cm^{-1} can be associated with the bending vibrations of asymmetrical H_2O molecules. The weak absorption peak at 1573 cm^{-1} may correspond to hydroxyl bending. The broad absorption peak appears between 420 cm^{-1} and 630 cm^{-1} are assigned to metal oxygen (M-O) stretching mode. The absorption band at 586 cm^{-1} corresponds to Fe-O stretching vibrations of Fe_3O_4. The prominent absorption peak observed in the range 490-590 cm^{-1} is the combination of Fe-O metal oxide vibrations [34, 35].

3.3 Scanning electron microscopy (SEM)

The surface morphologies of FENPs and FENRs samples were analyzed by high resolution scanning electron microscopy (HR-SEM). HR-SEM images of FENPs and FENRs samples for different magnification are shown in Fig. 3a-d and highly agglomerated to spherical shaped nanoparticles. Both nanoparticles (FENPs) and nanorods (FENRs) samples uniformly distributed with agglomeration. The occurrence of FENPs and FENRs might be attributed due to

the temperature effect during the reaction. Using energy- dispersive X-ray spectroscopy (EDX) the composition of each element present in the synthesized sample was established. The FENPs and FENRs consist of Fe and O elements which are clearly observed in Fig. 4 (a-b). The EDX spectrum confirms the presence of FENPs and FENRs samples without impurities.

3.4 UV-Visible spectrum analysis

The DRS optical absorption spectrums of the synthesized Fe_3O_4 nanoparticles (FENPs and FENRs samples) were measured using UV-vis spectrometer. Fig. 5 depicts the results of Kubelka-Munk (K-M) model and the F(*R*) is estimated using the formula, $F(R) = (1-R)^2/2R$, where F(*R*) is the Kubelka-Munk function, and *R*, is the reflectance. The extrapolation in the linear region of the plot gives an energy band gap E_g. The band gap energy of FENPs and FENRs samples is 2.1 eV and 1.9 eV respectively. The estimation of the optical absorption wavelength of the prepared samples is an essential factor for photocatalysis, sufficient electrons will be excited from valence band to the conduction band of the photocatalysts only if the energy of the incident light is equivalent to or greater than the photocatalysts band gap energy [36]. Otherwise the photocatalytic activity will not be effective. The UV-visible absorption results confirm that FENPs and FENRs samples can generate greater number of electrons and holes under UV light irradiation. It can also suggest that, during catalytic reactions, the generated holes and electrons will actively participate in oxidation and reduction process [37]. These results suggest that the photocatalytic efficiency of the FENPs and FENRs samples will be higher than that of the pure material.

3.5 Vibrating Sample Magnetometer Analysis

The magnetic hysteresis loops of the synthesized FENPs and FENRs samples were investigated by VSM with a magnetic field sweeping from -15 KOe to 15 KOe at room

temperature. The measured hysteresis loops of the sample are shown in Fig. 6. At low temperature, the magnetic moments of individual particles tend to orient along the field with an external magnetic field. When the temperature increases more and more particles reorient their magnetic moment along the applied field and the total magnetization increases [38]. Saturation magnetizations (Ms), Remanent magnetization (Mr) and Coercive field (Hc) are the main magnetic parameters of the VSM analysis listed in the Table 2. The magnetic saturation (Ms) of pure Fe_3O_4 is 65.4 emu/g. The saturation magnetization (Ms) value of the FENPs and FENRs samples are 45.56 emu/g and 37.25 emu/g respectively. It is shown that FENPs and FENRs samples exhibit ferromagnetic behavior with low saturation magnetization. But it is clearly observed that FENPs and FENRs samples exhibit good magnetic response for effective magnetic separation. The high coercivity (H_c) value of the samples corresponds to high surface anisotropy, which may attribute to high resonance frequency [39].

3.6 Photocatalytic Activity

The aim of the study is to degrade the organic pollutant (Methylene blue, MB). The photocatalytic activity of FENPs catalysts were carried out to find the most efficient catalyst among the prepared sample (FENRs). In this process MB dye is used as the model organic pollutant. In presence of UV irradiation, H_2O_2 plays vital role in degradation of MB as it generates two hydroxyl radicals (HO^*). The HO^* are considered extremely strong oxidant for the degradation of organic pollutants [40]. Thus, the incorporation of H_2O_2 helps in dye degradation. The decolouration of MB was monitored by the UV-Visible spectrometer. The disappearance of the band at 365 nm indicates that most of the MB has been degraded by the catalyst under UV light irradiation within 3h. The time dependent optical absorption spectra of MB with FENPs and FENRs samples a catalyst under UV light irradiation for different time intervals are shown in

Fig. 7. The impact on modified physical parameters such as reduced band gap, increased surface area plays a vital role in the degradation of dye, which generates hydroxyl groups in the process.

The amount of FENPs and FENRs samples was also found to affect the degradation process. The photocatalytic activity of the FENPs is higher because of the smaller crystallite size. The decrease in crystallite size increases the surface area. FENPs showed the effective phototcatalytic degradation of MB dye under UV light irradiation. The efficiency of the FENPs sample was 92 % than other sample (FENPs, 84 %). It is recognized that the photocatalytic redox reaction essentially happens on the surface of the catalyst thus the surface properties influence the efficiency of the catalyst. The morphology also acts as a possible feature that influences the final degradation efficiency [41]. The spherical shaped FENPs showed higher efficiency compared with other catalyst. The presence of Fe_3O_4 up to the optimum amount acts as an electron hole separation centre and hence enhances the photocatalytic activity. When the Fe_3O_4 content is greater than the optimum weight it acts as a charge-carrier recombination centre and hence reduces the efficient separation of charge [42].

During thephotocatalytic reaction, when the surface of FENPs and FENRs samples is irradiated with UV light, electrons in the valence band of Fe_3O_4 are excited because of its small band. The electrons then react with and absorb oxygen molecules to form superoxide radicals, which are responsible for the degradation/oxidation of the organic pollutant. The oxidation process is capable of decomposing organic pollutant under UV light and during the photocatalytic reaction, the recombination of the photogenerated electrons and holes can be prevented, which is helpful in improving the photocatalytic activity of the photocatalyst under light irradiation. FENPs exhibited greater degradation efficiency because of its narrow band gap

and wider absorption wavelength region, which resulted in the absorption of UV light and the production of more electrons and holes during the photocatalytic reaction.

3.7. Antibacterial Activities

The antibacterial activities of synthesized FENPs and FENRs samples were tested against the human pathogens like *Staphylococcus aureus*, *Proteus mirabilis*, S*almonella typhii* and *Bacillus subtilis* with reference to Ampicillin [43]. The inhibition zones of the FENPs and FENRs samples were shown in Figure 8 and the values are listed in Table 3. From the results, it was observed that the synthesized FENPs and FENRs samples showed desired activity against *P. mirabilis and S. typhi which causes* causes kidney stone and typhoid fever respectively. FENPs sample showed greater activity against *S. aureus and B. subtilis* than FENRs, which is mainly due to the higher surface area and surface to volume ratio [44, 45]. Hence, the synthesized FENPs and FENRs samples can be used as an antibacterial medicine.

4. Conclusion

In summary, we have synthesized FENPs and FENRs samples by simple combustion methods using ferric nitrate and Aloe vera extract as the raw materials. Powder XRD pattern reveals that formation of Fe_3O_4 structure. Magnetic studies confirm that FENPs and FENRs samples exhibits hysteresis loop. The observed different saturation magnetization of the FENPs and FENRs samples is mainly due to the difference in their grain size. The photocatalytic activity of the organic pollutant MB was studied and the efficiency of the samples was examined. Among the prepared samples, FENPs showed the effective phototcatalytic degradation of MB dye under UV light irradiation. The efficiency of the FENPs sample was 92 % than other sample (FENPs, 84 %). The results were in agreement with various characterization techniques. The factors used to increase the degradation efficiency are specific surface area of the catalyst, optimum

dispersion of Fe_3O_4 nanoparticles and surface defects. Also used as a reusable photocatalyst for at least three to four cycles with little change in its activity.

References

[1] E. Comini, C. Baratto, G. Faglia, M. Ferroni, A. Vomiero, G. Sberveglieri, Prog. Mater. Sci., 54, 1 **(2009).**

[2] N. Bayal, P. Jeevanandam, Mater. Res. Bull., 48, 3790 **(2013).**

[3] Y. He, Lihong Zhang, M. Fan, X. Wang, Mikel L. Walbridge, Q. Nong, Y. Wu, L. Zhao, Solar Energy Mater. Solar Cells, 137, 175 **(2015).**

[4] K. Ikehata, N.J. Naghashkar, M, Gamal El-Din**,** Ozone Sci. Eng., 28, 353 **(2006).**

[5] D. Singh, S. Verma, R. K. Gautam, V. Krishna**,** J. Environ. Chem. Eng., 3, 2161 **(2015).**

[6] S. W. Cao, Y. J. Zhu, M. Y. Ma, L. Li, L. Zhang, J. Phys. Chem. C, 112, 1851 **(2008).**

[7] Y. F. Zhu, W. R. Zhao, H. R. Chen, J. L. Shi, J. Phys. Chem. C, 111, 5281 **(2007).**

[8] L. Josephson, C. H. Tsung, A. Moore, R. Weissleder, Bioconjugate Chem., 10, 186 **(1999).**

[9] P.V. Kamat, J. Phys. Chem. C, 111, 2834 **(2007).**

[10] Z.W. Chen, Z. Jiao, M.H.Wu, C.H. Shek, C.M.L.Wu, J.K.L. Lai, Prog. Mater. Sci., 56, 901 **(2011).**

[11] M. Batzill, U. Diebold, Prog. Surf. Sci. 79, 47 **(2005).**

[12] Y. Han, X. Wu, Y. Ma, L. Gong, F. Qu, H. Fan, Cryst. Eng. Comm, 13, 3506 **(2011).**

[13] D. Chu, J. Mo, Q. Peng, Y. Zhang, Y. Wei, Z. Zhuang, Y. Li, Chem. Cat. Chem., 3, 371 **(2011).**

[14] S. Wu, H. Cao, S. Yin, X. Liu, X. Zhang, J. Phys. Chem. C, 113, 17893 **(2009).**

[15] T. Xin, M. Ma, H. Zhang, J. Gu, S. Wang, M. Liu, Q. Zhang, App. Surf. Sci. 288, 51 **(2014).**

[16] Z. Wang, Y. Du, F. Zhang, Z. Zheng, X. Zhang, Q. Feng, C. Wang, Mater. Chem. Phys., 140, 373 **(2013).**

[17] A. F. Shojaei, A. S.Nateri, M. Ghomashpasand, Superlat. Microstruct. 88, 211 **(2015).**

[18] R. Chen, J. Cheng, Yu Wei, J. Alloys Compd. 520, 266 **(2012)**.

[19] M. Srivastava, J. Singh, M. Yashpal, D.K. Gupta, R. K. Mishra, S. Tripathi, A.K. Ojha, Carbohydrate Polym. 89, 821 **(2012)**.

[20] A. Roychowdhury, S.P.Pati, A.K.Mishra, S.Kumar, D.Das, J. Phys. Chem. Solids 74, 811 **(2013)**.

[21] Q. Zhang, M.F. Zhu, Q.H. Zhang, Y.G. Li, H.Z. Wang, Compos. Sci. Technol. 69, 633 **(2009)**.

[22] T. Reynolds, A.C. Dweck, Aloe vera leaf gel: a review update, J. Ethnopharmacol. 68, 3 **(1999)**.

[23] K. H. Shin, W. S. Woo, S. S. Lim, C. S. Shim, H. S. Chung, E. J. Kennely, A. D. Kinghorn, J. Nat. Prod. 60, 1180 **(1997)**.

[24] K. Umano, K. Nakahara, A. Shoji, T. Shibamoto, J. Agric. Food Chem. 47, 3702 **(1999)**.

[25] D. Saccu, P. Bagoni, G. J. Procida, J. Agric. Food Chem. 49, 4526 **(2001)**.

[26] S. P. Chandran, M. Chaudhary, R. Pasricha, A. Ahmad, M. Sastry, Biotechnol. Prog. 22, 577 **(2006)**.

[27] S. Maensiri, P. Laokul, J. Klinkaewnarong, S. Phokha, V. Promarak, S. Seraphin, J. Optoelectron. Adv. Mater.10, 161 **(2008)**.

[28] S. Phumying, S. Labuayai, E. Swatsitang, V. Amornkitbamrung, S. Maensiri, Mater. Res. Bull. 48, 2060 **(2013)**.

[29] J. Klinkaewnarong, E. Swatsitang, C. Masingboon, S. Seraphin, S. Maensiri, Curr. Appl. Phys. 10, 521 **(2010)**.

[30] P. Laokul, S. Maensiri, J. Optoelect. Adv. Mater. 11, 857 **(2009)**.

[31] P. Laokul, V. Amornkitbamrung, S. Seraphin, S. Maensiri, Curr. Appl. Phys. 11, 101 **(2011)**.

[32] D. Zhang, X. Zhang, X. Ni, J. Song, H. Zheng, Cryst. Growth Des. 7, 2117 **(2007)**

[33] M. Srivastava, J. Singh, M. Yashpal, D. K. Gupta, R. K. Mishra, S. Tripathi, A.K. Ojha, Carbohydrate Polym. 89, 821 **(2012)**

[34] O. Rahman, S. C. Mohapatra, S. Ahmad, Mater. Chem. Phys. 132, 196 **(2012)**

[35] Z. Cheng, Z. Gao, W. Ma, Q. Sun, B. Wang, X. Wang, Chem. Eng. J. 209, 451 **(2012)**

[36] M. B. Sahana, C. Subakar, G. Setzler, A. Dixit, J. S. Thakur, G. Lawes, R.Naik, Appl. Phys. Lett. 93, 231909 **(2008)**

[37] H. Zhuang, J. Wang, H. Liu, J. Li, P. Xu, Acta Phys. Polonica A 119, 819 **(2011)**

[38] J. Joseph, K. K. Nishad, M. Sharma, D. K. Gupta, R. R. Singh, Pandey, Mater. Res. Bull. 47, 1471 **(2012)**

[39] Y. Wei, B. Han, X. Hu, Y. Lin, X. Wang, X. Deng, Procedia Eng. 27, 632 **(2012)**

[40] S. R. Ali, P. Chandra, M. Latwal, S. K. Jain, V. K. Bansal, S. P. Singh, Chin. J. Catal. 32, 1844 **(2011)**

[40] M. Mousavi, A. H. Yangjeh, Mater. Res. Bull. 105, 159 **(2018)**

[41] Y. Chen, X. Jin, P. Guo, J. Mol. Struct., 1171, 140 **(2018)**

[42] M. S. Gohari, A. H. Yangjeh, Ceram. Int. 43, 3063 (**2017**)

[43] R. Bomila, S. Srinivasan, S. Gunasekaran, A. Manikandan, J. Supercond. Nov. Magn. 31, 855 (**2017**).

[44] A. Manikandan, E. Manikandan, B. Meenatchi, S. Vadivel, S. K. Jaganathan, R. Ladchumananandasivam, M. Henini, M. Maaza, J. S. Aanand, J. Alloys Compds. 723, 1155 (**2017**).

[45] A. T. Ravichandran, J. Srinivas, Karthick, A. Manikandan, A. Baykal, Ceram. Int. 44, 13247 (**2018**).

Figures

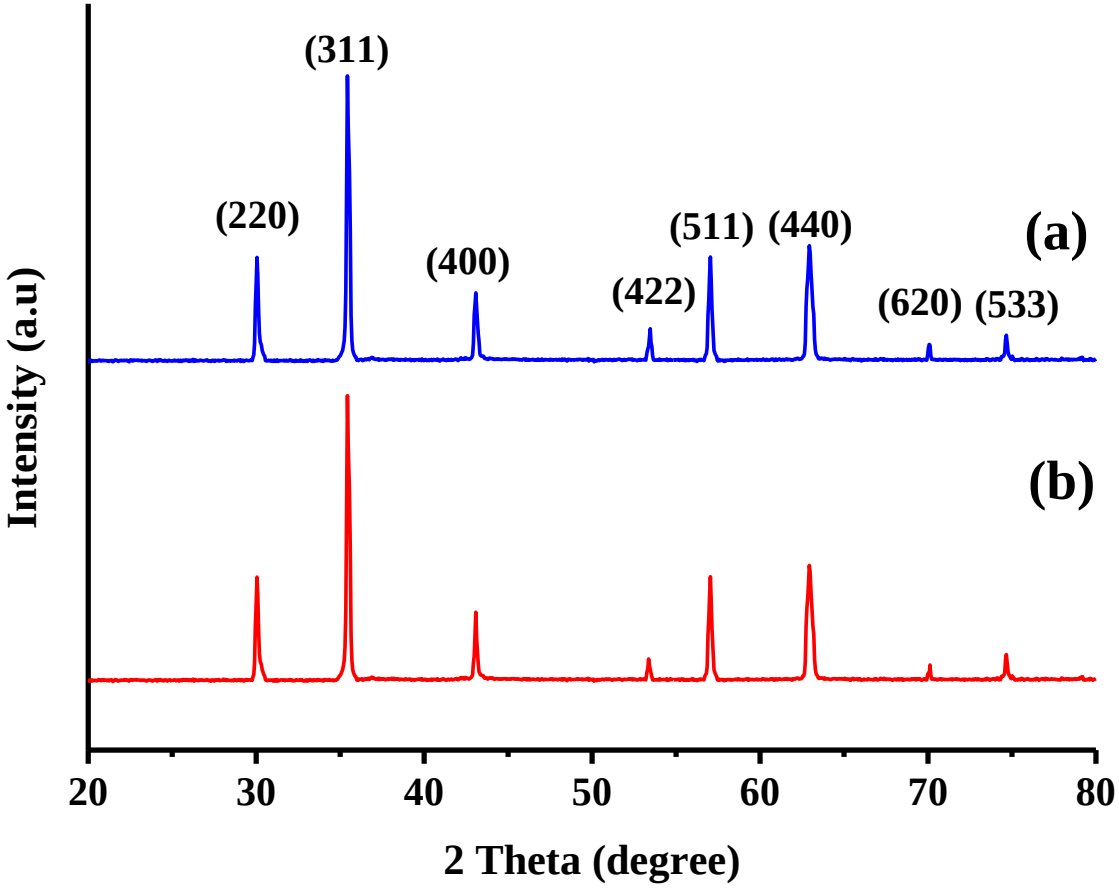

Fig. 1. XRD pattern of (a) FENPs and (b) FENRs samples.

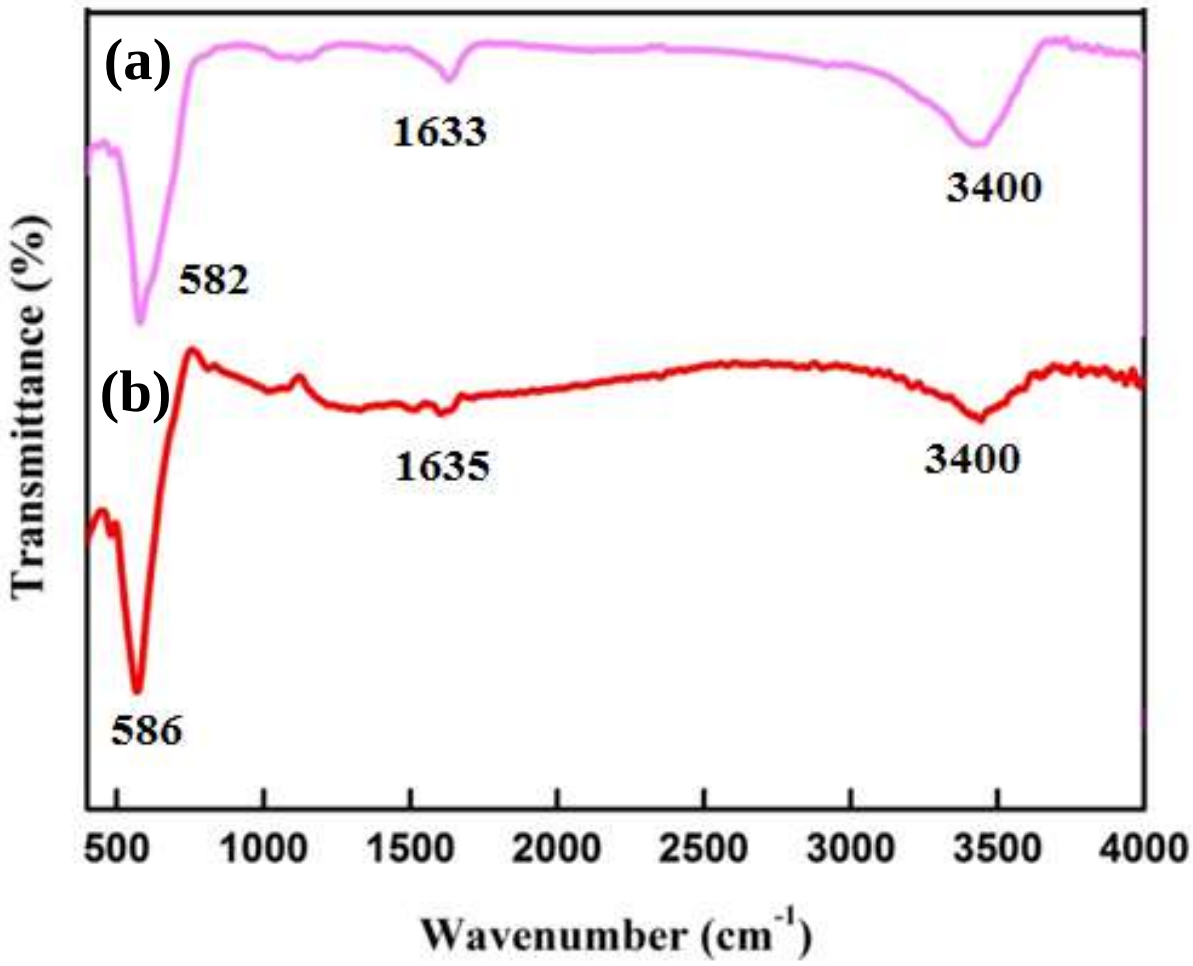

Fig. 2. FTIR analysis of FENPs and FENRs samples.

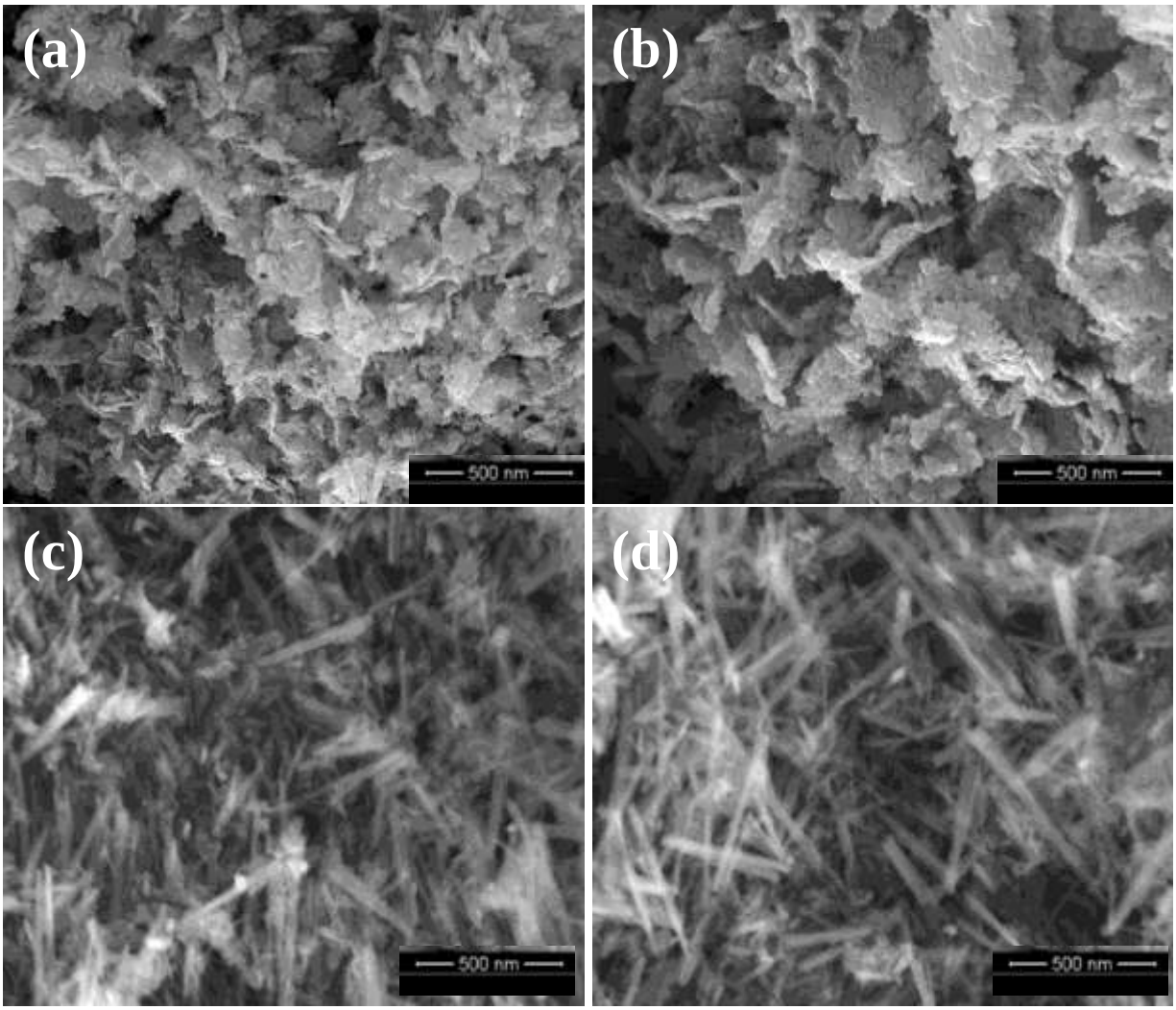

Fig. 3. HR-SEM images of FENPs (a, b) and FENRs (c, d) samples.

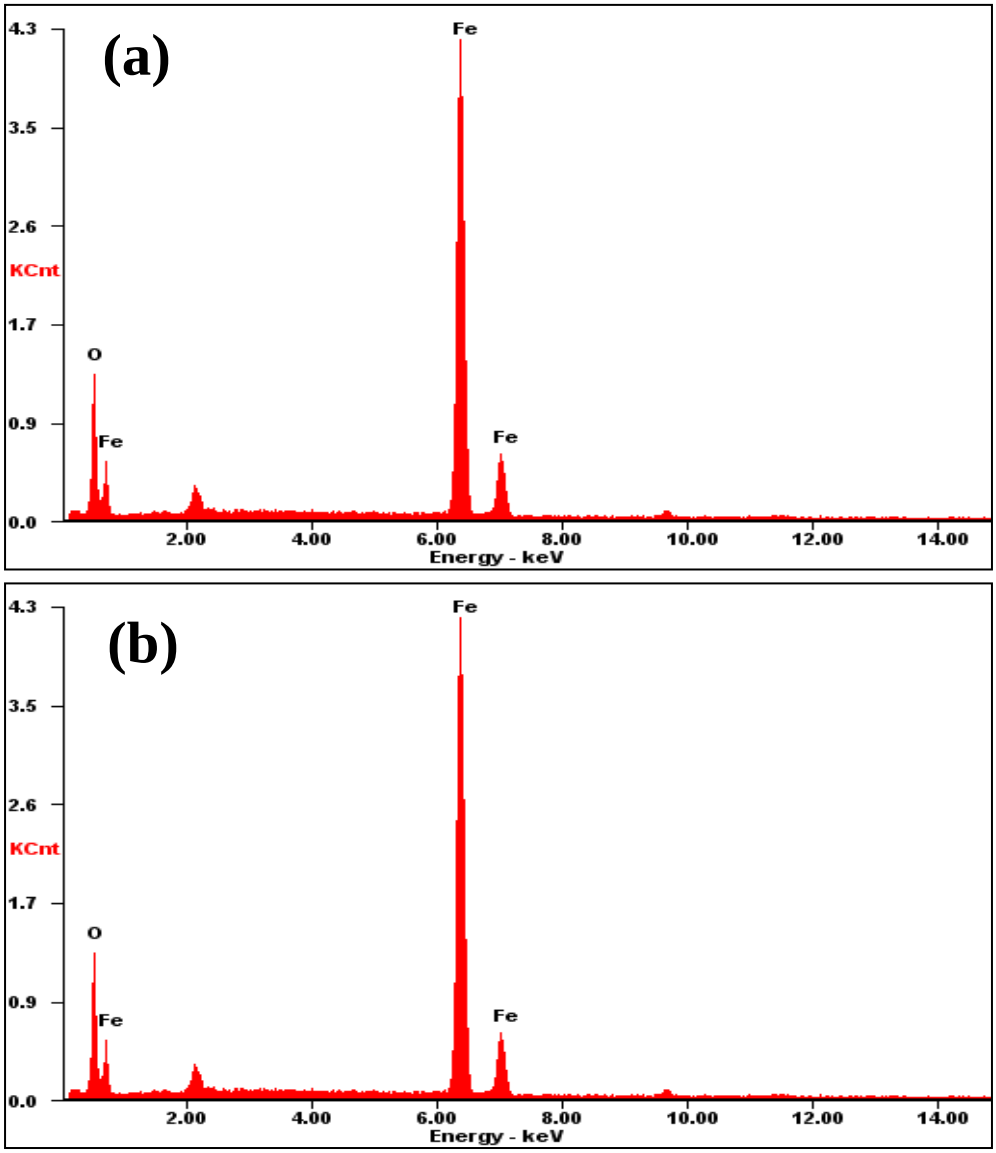

Fig. 4. EDX spectra of FENPs (a) and FENRs (b) samples.

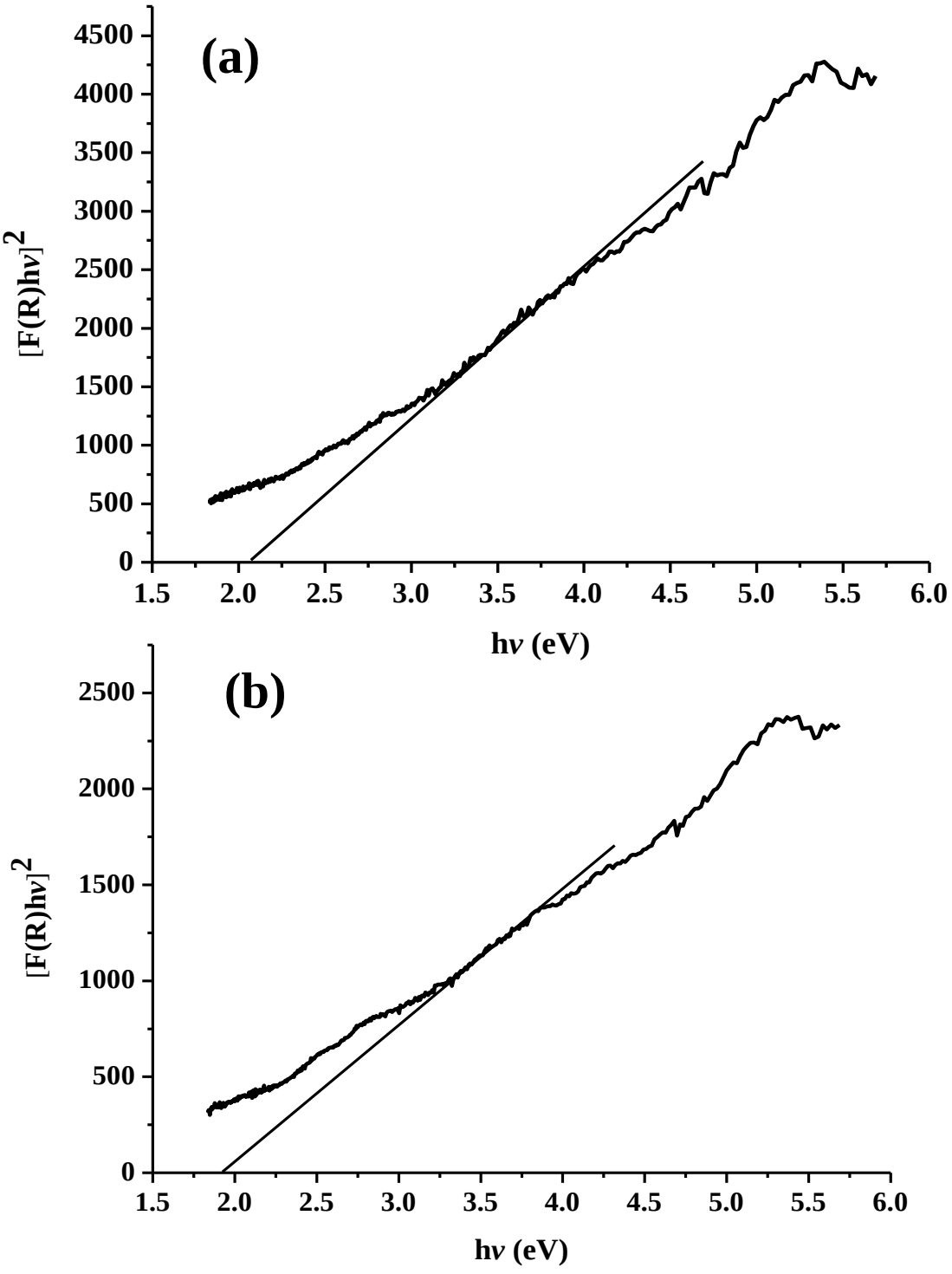

Fig. 5. UV-Vis DRS spectra of FENPs (a) and FENRs (b) samples.

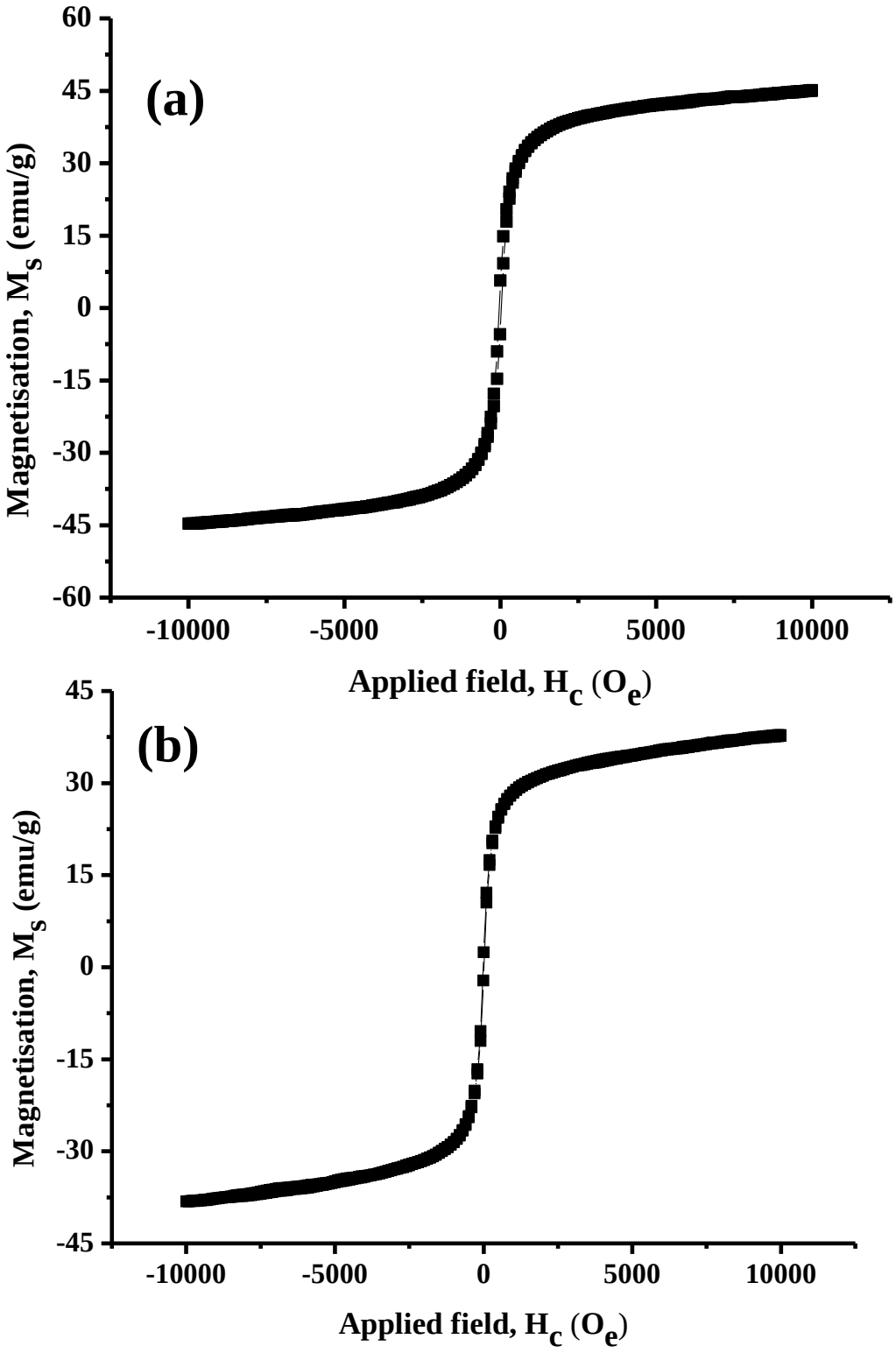

Fig. 6. Room temperature VSM results of FENPs (a) and FENRs (b) samples.

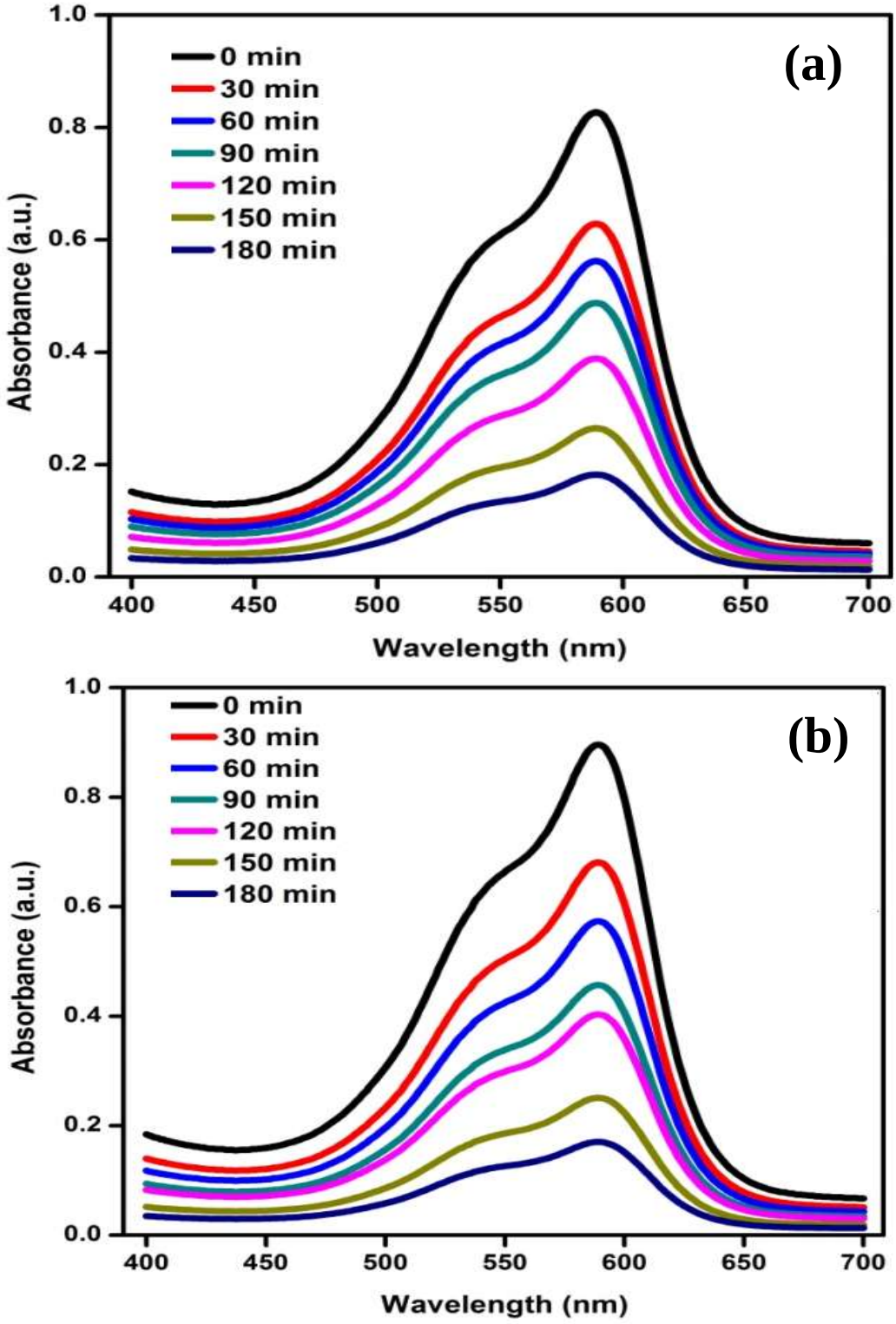

Fig. 7. Photocatalytic degradation of methylene blue under UV light irradiation FENPs (a) and FENRs (b) samples.

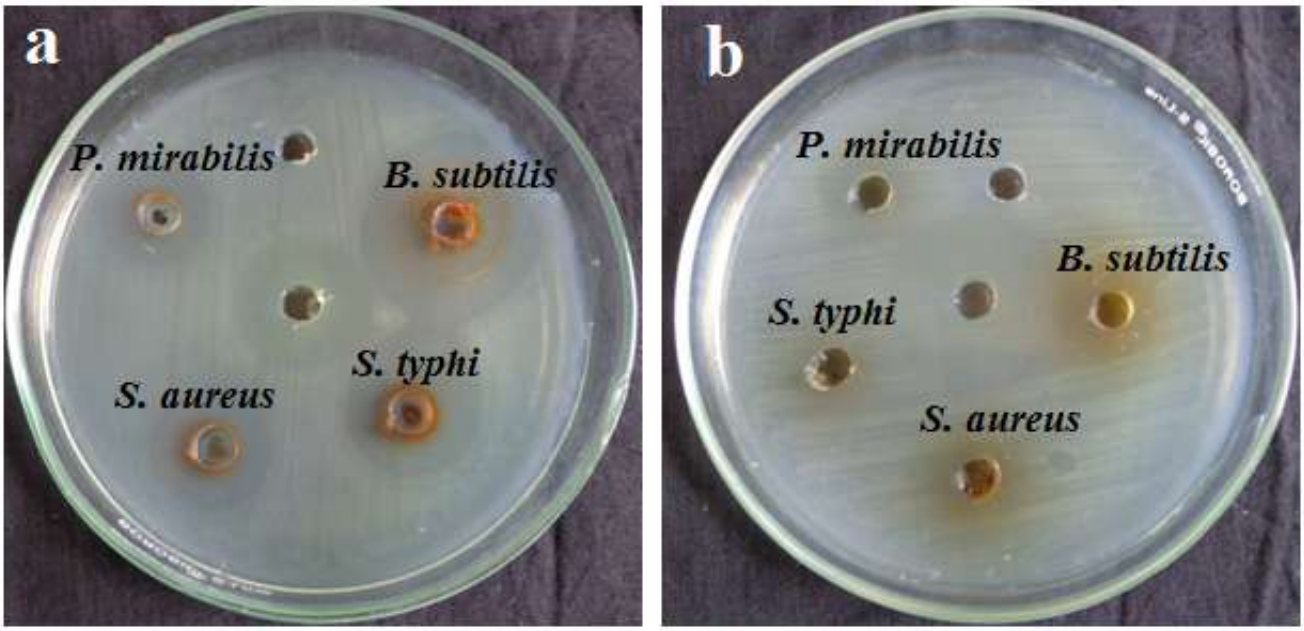

Figure 8. Antibacterial activity of FENPs (a) and FENRs (b) samples.

Tables:

Table1. Crystallite Size and Lattice parameters of FENPs and FENRs samples

Samples Code	Crystallite Size (nm)	Fe_3O_4 cubic a (Å)	Band gap (eV)
FENPs	23.85	8.328	2.1
FENRs	32.54	8.331	1.9

Table 2. Coercivity (Hc), Retentivity (Mr) and Magnetization (Ms) parameters of FENPs and FENRs samples obtained from room temperature VSM measurements.

Samples	Saturation Magnetization (M_s) (emu/g)	Coercivity (H_{ci})	Retentivity (M_r) (emu)	Squareness ratio (M_r/M_s)
FENPs	**45.56**	**122.5**	**1.0236**	**0.027**
FENRs	**37.25**	**126.4**	**1.0312**	**0.022**

Table: 3 Antibacterial activities of FENPs and FENRs samples for against human pathogens.

Antibacterial activities of samples were determined as zone of inhibition (in mm)				
Samples	***P. mirabilis***	***S. typhi***	***S. aureus***	***B. subtilis***
Ampicillin (C)	**19**	**16**	**12**	**14**
FENPs	**6**	**11**	**13**	**23**
FENRs	**5**	**8**	**10**	**18**